SP2016_3124639

COMPARISON OF OXYGEN-HYDROGEN COMBUSTION VISUALISION TECHNIQUES UNDER REPRESENTATIVE CONDITIONS

S. Webster[(1)], J. Hardi[(1)], M. Oschwald[(1,3)].
[(1)]DLR- German Aerospace Centre, Institute of Space Propulsion, Lampoldshausen, Germany, D-74239, Email: samuel.webster@dlr.de,
[(2)]RWTH Aachen University, Aachen, Germany, D-52062

KEYWORDS: liquid propellant rocket engine, combustion instability, optical diagnostics, flame visualisation, cryogenic propellants

ABSTRACT:

Flame behaviour when exposed to acoustic excitation is investigated using the visible spectrum imaging technique. Two acoustic conditions are examined; flame behaviour during rapid growth, and during constant high amplitude pressure oscillations. These conditions are representative of combustion instability onset and limit cycle conditions, respectively. Visible imaging is compared to the widely used OH* imaging technique to characterise its use for combustion instability applications. The development of increased mixing and contraction of the central jet due to transverse excitation was observed for combustion instability conditions. The response of the flame to the pressure growth was rapid showing significant changes over less than five acoustic periods. The influence of transverse velocity on the flame was also observed for limit cycle conditions.

1. INTRODUCTION

Thermo-acoustic combustion instabilities, commonly referred to high frequency combustion instabilities, present an ongoing risk to rocket combustion engine operation [1]. Combustion instabilities are characterized by the rapid onset of high amplitude pressure oscillations at combustor eigenmode frequencies. These pressure oscillations can change the operational behaviour resulting in the destruction of the combustor. A significant amount of research has been undertaken since combustion instabilities were first identified [2]. However, more work is required to fully understand the phenomenon so that the risk of combustion instability onset can be mitigated.

Combustion instabilities are driven by coupling between the acoustic field and the flame. Only a small percentage of the available chemical energy must be transferred into the acoustic field to drive high amplitude oscillations. The addition of this energy must be in phase with the acoustic pressure field. The requirement for energy addition into the acoustic field and combustion instability onset is described by the Rayleigh criterion;

$$\int_V \int_T P'(x,t)Q'(x,t)dtdv \geq \Gamma \qquad (1)$$

where P' is the fluctuating pressure, Q' is the fluctuating heat release and Γ represents the damping of the system. This is a modified form of the Rayleigh criterion presented in [3] and focuses on energy addition.

To better understand the energy feedback mechanisms which drive self-sustained instability, a number of experimental combustors have been developed which have the capability to simulate combustion instability and study the flame behaviour [4-8]. These combustors work by imposing an acoustic field on the combustor through the opening and closing of a nozzle. Because the acoustic field is imposed, flame-acoustic interaction can be investigated in a controlled environment. Understanding how the acoustic field couples with and changes flame behaviour is critical to the understanding of combustion instabilities.

Using cameras with high acquisition rates, flame radiation imaging has been used to study combustion instabilities [8-11]. In combination with shadowgraph imaging and pressure field information these studies provide insight into flame-acoustic interactions and are a valuable dataset for validation of numerical simulation.

The propellant combination oxygen-hydrogen is widely used in rocket engines due to its high specific impulse. Visualisation of oxygen-hydrogen flames has traditionally been made with filtered OH radical (OH*) chemiluminescence measurement techniques as outlined by [12,13]. More recently these techniques have been applied to conditions representative of flight rocket engines [14,15]. However, OH* imaging presents additional challenges at high temperatures and pressures such as those observed in liquid propellant rocket combustion chambers. The OH radical is strongly thermally excited, with thermal emissions dominating contributions from chemiluminescence at temperatures above 2400 K [16]. Radiation from OH* is also readily absorbed and consequently has a low mean free path. This provides additional challenges in flame imaging where an integrated

[1] Corresponding author:
Phone: +49 6298 28 427
Email: samuel.webster@dlr.de

line of sight measurement, as opposed to a surface measurement, may be sought.

Recent investigations into the applicability of OH* emission at high temperatures and pressures have been undertaken [17-20]. As part of these investigations it was found that there was a spatial inconsistency between chemical reaction and emission from OH* which was attributed to thermal excitation as the primary emission mechanism at high pressures. A continuous emission spectrum peaking at 440 nm, termed 'blue radiation', was also investigated. The source of blue radiation may be connected to the chemiluminescence of H_2O_2*, which is a radical that is not thermally excited [19]. Additionally, blue radiation was not readily reabsorbed, producing an increased depth of view when compared to OH* emissions.

In this investigation both broad band visible imaging (VIS), which includes the blue radiation band, and more traditional OH* imaging are employed to investigate acoustic-flame interactions. The flame response under two different acoustic conditions is investigated. The first condition is representative of instability onset with rapidly growing pressure amplitudes. The second is representative of flame behaviour under limit cycle conditions. The flame behaviour under the two conditions is compared and discussed.

2. EXPERIMENTAL APPARATUS

2.1. Combustion chamber

Flame visualisation experiments were conducted at the German Aerospace Center's test bench for high pressure cryogenic research, 'P8', using the combustor 'BKH'. BKH has a rectangular cross section with the dimensions outlined in Figure 1. The dimensions were selected to be consistent with upper stage flight engines as representative eigenmode frequencies are considered important for combustion instability investigations [21].

BKH is equipped with optical access windows to visualise the flame, originating from the primary injector, in the near injection region. In addition to the main nozzle, BKH is equipped with a secondary nozzle. The secondary nozzle, located at the top of the combustor, can be opened and closed with a siren wheel to impose an acoustic field on the combustor volume. Two siren wheels were used in this investigation, a sector wheel that periodically excites combustor acoustics, and the full wheel which continuously excites combustor acoustics. The outlet area of the secondary nozzle is 9% that of the main nozzle which is not modulated.

The combustor is also equipped with dynamic pressure sensors, distributed along the combustor walls, which allow for identification of chamber modes and reconstruction of the acoustic pressure field. The sensors used in this investigation were flush-mounted Kistler type 6043A60 which have an accuracy of ±0.04 bar when set to measure pressure oscillations of up to ±20 bar. The pressure was sampled at a rate of 100 kHz and a 30 kHz anti-aliasing filter was applied.

The operating conditions used in this investigation are given in Table 1.

2.2. Propellants and Injection

BKH has three main injection zones. The primary injector, the secondary injector and the window film cooling injector. The location of these can be seen in Figure 1.

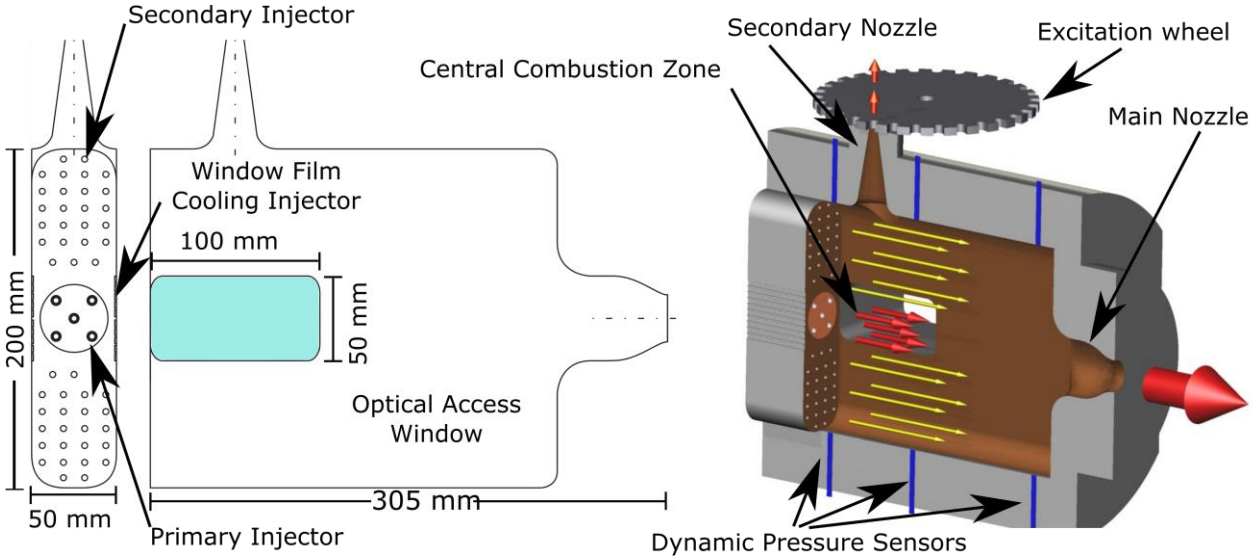

Figure 1: Illustration and dimensions of combustor BKH

The primary injector consists of 5 shear-coaxial injectors in a matrix pattern. Cryogenic oxygen is injected through the central annulus and cryogenic hydrogen through the outer. The dimensions of the primary injector are given in Figure 2.

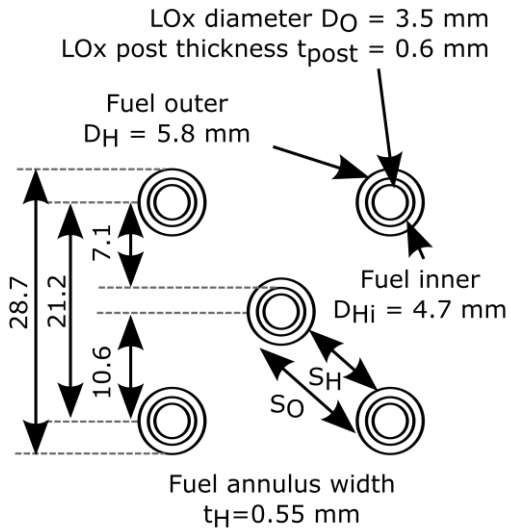

Figure 2: Primary injector dimensions

The secondary injector located above and below the primary injector, injects ambient temperature hydrogen through 50 simple orifice injection elements with an outlet diameter of 3.5mm. The secondary injector was designed to limit the recirculation zones by providing a co-flow to the primary injection element. Additionally, the secondary hydrogen protects the secondary nozzle and upper and lower walls from hot combustion products.

The window film cooling injector is located either side of the primary injector. Ambient temperature hydrogen is injected to protect the optical access windows from the combustion zone.

2.3. Optical Diagnostic Configuration

In this configuration up to three cameras were used to visualise combustion in BKH. Two cameras were used to measure OH* intensity, one on axis and one off axis. One camera was used to measure visible spectrum (VIS) intensity. The configuration of the cameras around the combustion chamber is shown in

Figure 3.

The on-axis, high-speed, intensified OH* camera and the high-speed, visible imaging (VIS) camera obtained parallel imaging of the flame through the use of a dichroic mirror. Consequently, due to the reflection of OH* by the mirror no OH* emission was measured by the VIS camera. The on-axis OH* camera had not been used during previous campaigns and so for comparison purposes the off-axis camera was used for this investigation.

VIS does not employ a wave length filter and so captures a range of the emission spectrum based on the camera response. Importantly, VIS captures the blue radiation band improving the flame penetration of the camera.

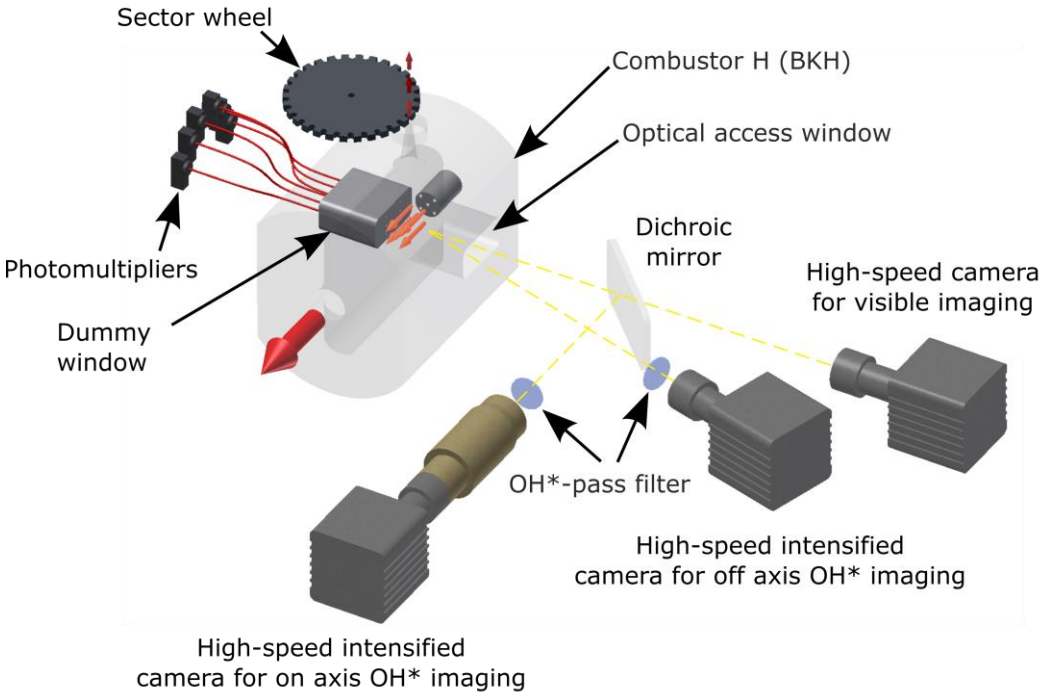

Figure 3: Camera configuration around BKH

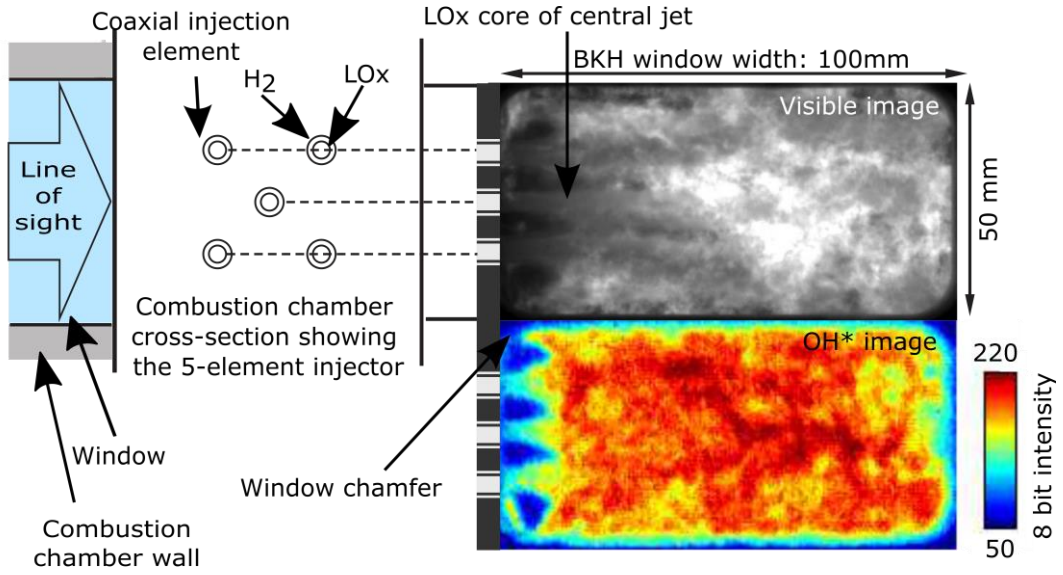

Figure 4: Line of sight measurements

Table 1: Combustion chamber operating conditions

Operating condition	Periodic excitation	Continuous excitation
Pressure (Pcc)	40 bar	40 bar
Oxidiser to Fuel Ratio (ROF)	6	6
Hydrogen Temperature	49 K	64 K
Oxygen Temperature	120 K	120 K

The cameras capture integrated line-of-sight measurements of the flame. This line of sight is from the side of the combustor with all five injection elements visible. Figure 4 shows an example of the integrated line-of-sight, on-axis, measurements of OH*, in false colour, and VIS image, in greyscale

Imaging along the same optical axis was not available for all test cases so a comparison of on and off axis imaging is required. Figure 5 provides the comparison between on-axis VIS imaging and off-axis OH* imaging for the on resonance condition. The distribution of the flame for both optical axes is well captured. However, due to parallax, the length position marker shifts relative to the flame making spatial comparison of the flames more challenging. The two position markers labelled in Figure 5 are the same, and their position shows the relative parallax effect against the background flame.

The camera and settings for each experiment are given in Table 2. The images were post processed to improve the identification of flame phenomenology. For presentation purposes all images were post processed with a brightness of +0.68 and gamma of 1.1935.

Table 2: Camera settings

Settings	Periodic excitation	Continuous excitation
OH* Camera	Ultima APXi2	Ultima APXi2
VIS Camera	Fastcam SA5	Fastcam SA5
OH* Intensifier Gating (μs)	0.35	0.35
OH* Frame Rate (fps)	30,000	6,000
OH* Resolution (pixel)	446±22	228±40
VIS Shutter Speed (μs)	0.400	0.404
VIS Frame Rate	20,000	30,000
VIS Resolution(μm/pixel)	154±8	178±8

3. RESULTS

3.1. Flame Phenomenology

The flame phenomenology of both the OH* and VIS emissions were compared during high amplitude excitation. The purpose of the comparison was to characterise the flame distribution and optical depth for the not widely applied VIS imaging when compared to the well-established OH* visualisation technique.

Figure 5 shows synchronised single image frames of VIS and OH* imaging mirrored around the central axis of the window. The flame extends about two thirds the length of the combustion chamber. Similar flame topology can be seen in both the OH* and in the VIS imaging. However, the regions of high intensity corresponding to the combustion zone around the central oxygen jet are more distinguished in the VIS imaging, owing to the generally stronger intensity gradients within the flame region. The OH emissions appear to be more homogeneous and distributed down the combustor length.

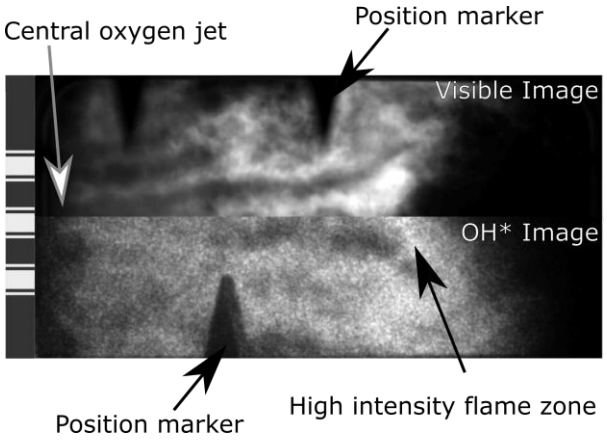

Figure 5: Comparison of Vis, image a, and OH, image b, on-resonance*

The mean intensities of over 33 ms for VIS and OH* are presented in Figure 6. In this study, the dichroic mirror acts as a stop band filter for the emission from OH*. Therefore, when comparing the images in Figure 6 the emission contributions are separated.

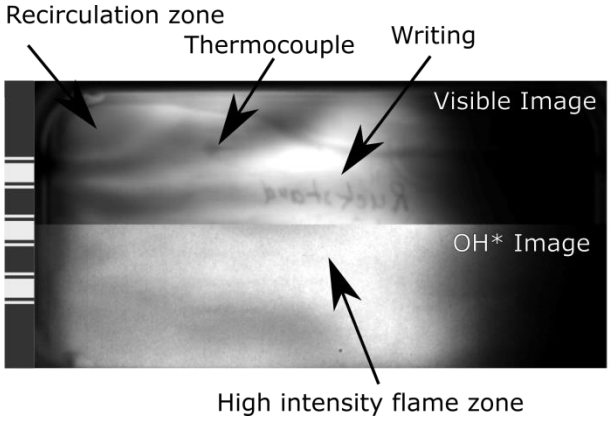

Figure 6: Mean intensity images of, image a, VIS emission and image b, OH emission*

The VIS image shows an optically thin flame with writing and thermocouples visible on the back wall. In the OH* image these features are not visible suggesting a greater optical thickness of the flame at this wave length. The optical depth of VIS when compared to OH* in Figure 6 is much higher. This is consistent with observations made in literature with single laminar laboratory flames where OH* optical depth was observed to relate strongly with temperature and pressure [18]. The overall flame structure is comparable in the two images although OH* emissions are again more homogeneously distributed than VIS emissions.

The following sections focus on VIS imaging to compare the dynamic flame response under the two acoustic conditions; rapid amplitude growth and established limit cycle conditions.

3.2. Visible imaging of flame response to variable amplitude acoustic excitation

Variable amplitude excitation, through the use of a sector wheel, is representative of combustion instability onset. During combustion instability onset acoustic amplitudes rapidly grow before a limit cycle is reached. The periodic excitation of the sector wheel produces a rapid amplitude growth during the excitation phase before excitation ceases and the amplitude is allowed to decay. This allows the influence of pressure growth on flame structure and the rapidity of flame response to transient acoustic conditions to be investigated. The results presented here are a summary of earlier work which is made for later comparison with continuous excitation [22].

Figure 7 and Figure 8 show the response of pressure and image intensity, respectively, to periodic excitation of the first transverse mode. The mean image intensity of both cameras as well as the mean chamber pressure appear to lag dynamic pressure amplitude. However, the time lag appears to be less than a quarter period.

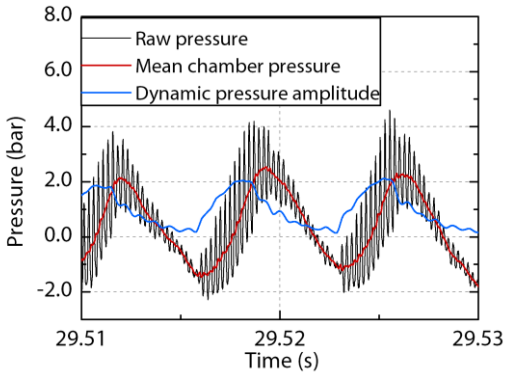

Figure 7: Periodic response of pressure to sector wheel excitation

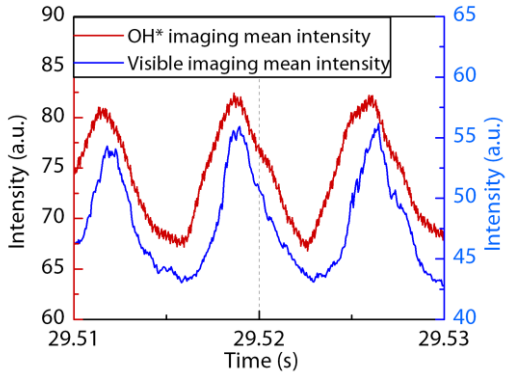

Figure 8: Periodic response of image intensity to sector wheel excitation

To examine this behaviour more closely, images corresponding to one cycle of mean intensity fluctuation were selected. Figure 9 shows the time of the points of the images selected. Figure 10 shows, in series, the 5 images selected.

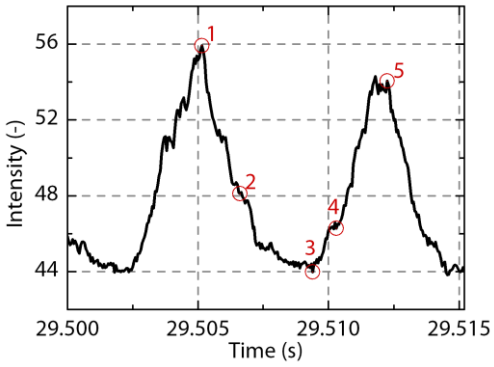

Figure 9: Selection of images for Figure 10 with respect to mean intensity fluctuation

The first and the last images occur at the point of maximum intensity. This point also corresponds to the point of maximum pressure amplitude. The images selected at points 2, 3 correspond to a period of decreasing pressure amplitude. Image 4 is taken as the pressure amplitude and mean intensity are increasing.

As the amplitude of pressure oscillation increases (points 4 to 5), regions of high emission intensity appear along either side of the central jet. The regions of high intensity appear downstream and as amplitude increases, they progress upstream, toward the faceplate. This behaviour is attributed to increased mixing due to transverse velocity oscillations. When the pressure amplitude is allowed to decay (Points 1 to 3), the regions of high intensity are convected downstream.

The oxygen jets are clearly visible and show up as darker regions with regions of high intensity on either side, such as in Figure 6 and Figure 10. A polished steel dummy window was used on the back side of the chamber which has an unknown influence on the image. Future investigations will have to consider the role of reflected light on the dynamic behaviour observed using VIS imaging.

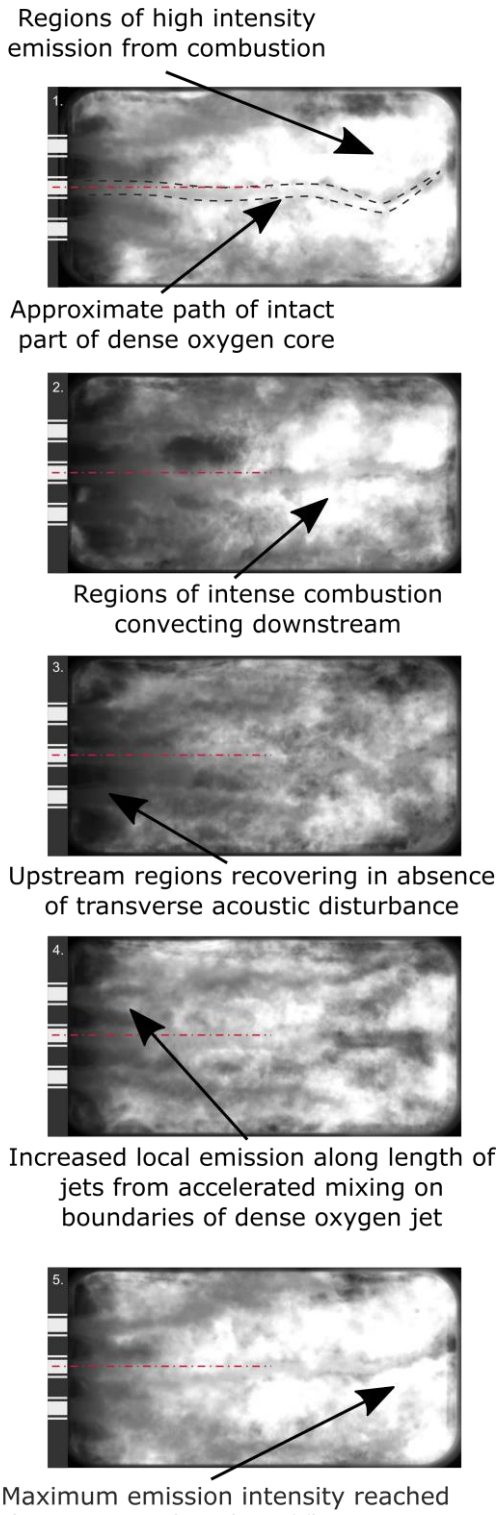

Figure 10: VIS imaging of flame response to variable amplitude excitation.

The response of the jet to growing pressure amplitudes was rapid, showing a considerable change in flame phonology over less than five acoustic cycles. The contraction of the flame toward the faceplate increases the amount of

energy available to couple with the acoustic field at that location. This redistribution of energy release during instability onset should be taken into account in predictive models of rocket engine stability.

Visualisation of the flame response to variable amplitude excitation provides a unique dataset for the validation of numerical models. Time domain CFD simulations of combustion instability onset under representative conditions could be compared with such visualisation. Furthermore, nonlinear effects arising from the redistribution of energy release and their contribution to limit cycle amplitudes could be determined.

3.3. Visible imaging of flame response to constant amplitude acoustic excitation

The full wheel was used to investigate the influence of constant amplitude excitation on the central combustion zone. For comparison, the operating conditions were kept the same as for the periodic excitation case (Table 1).

Excitation amplitudes of 6 bar peak-to-peak were reached. Figure 11 shows the pressure oscillations during maximum amplitude 1T-mode excitation. Nine time points corresponding to the acquisition of instantaneous VIS images were selected for further investigation. At each of these time points the pressure and velocity fields were reconstructed by interpolating between 6 dynamic pressure sensor measurements which were distributed in the upper and lower walls as seen in Figure 1. Figure 11 shows the pressure and velocity field reconstruction for time point 1.

To investigate the influence of the acoustic field on the flame, the localised velocity field in the window region was compared to the VIS imaging frames at points 1 to 9. Figure 12 shows a series of 9 figures split into three columns. The first column shows the velocity field in the window region. The second shows the VIS image at the same instance. The third column is a zoomed sub-image of the near injection region as defined by the blue box in the second column at time point 1. For both time points 2 and 3 the central axis of injection is shown by a dashed red line.

In the right hand column, regions of high intensity can be seen alternately above or below the central injection axis. The location, above or below, appears to be dependent on the direction of the velocity field. However, the areas of high intensity also appear to lag the velocity field. For example, at point 4, velocity is at its maximum in the upward direction whereas the emission intensity above the central axis reaches its peak at point 5, around 5×10^{-5} s or 20% of a 1T mode pressure cycle later. This suggests that the central jet does not react immediately to the velocity field. The delay corresponds to less than one frame. Consequently, the delay cannot be measured precisely; however, it was estimated to be around 45°. A more precise analysis of this phase relationship is currently in progress.

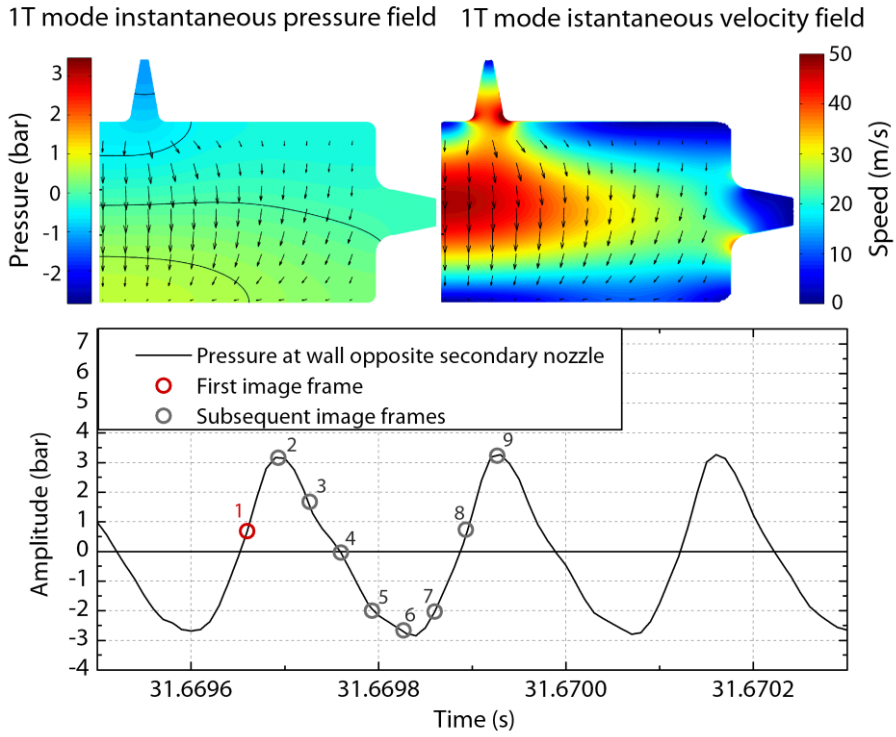

Figure 11: Typical test run with key operating conditions.

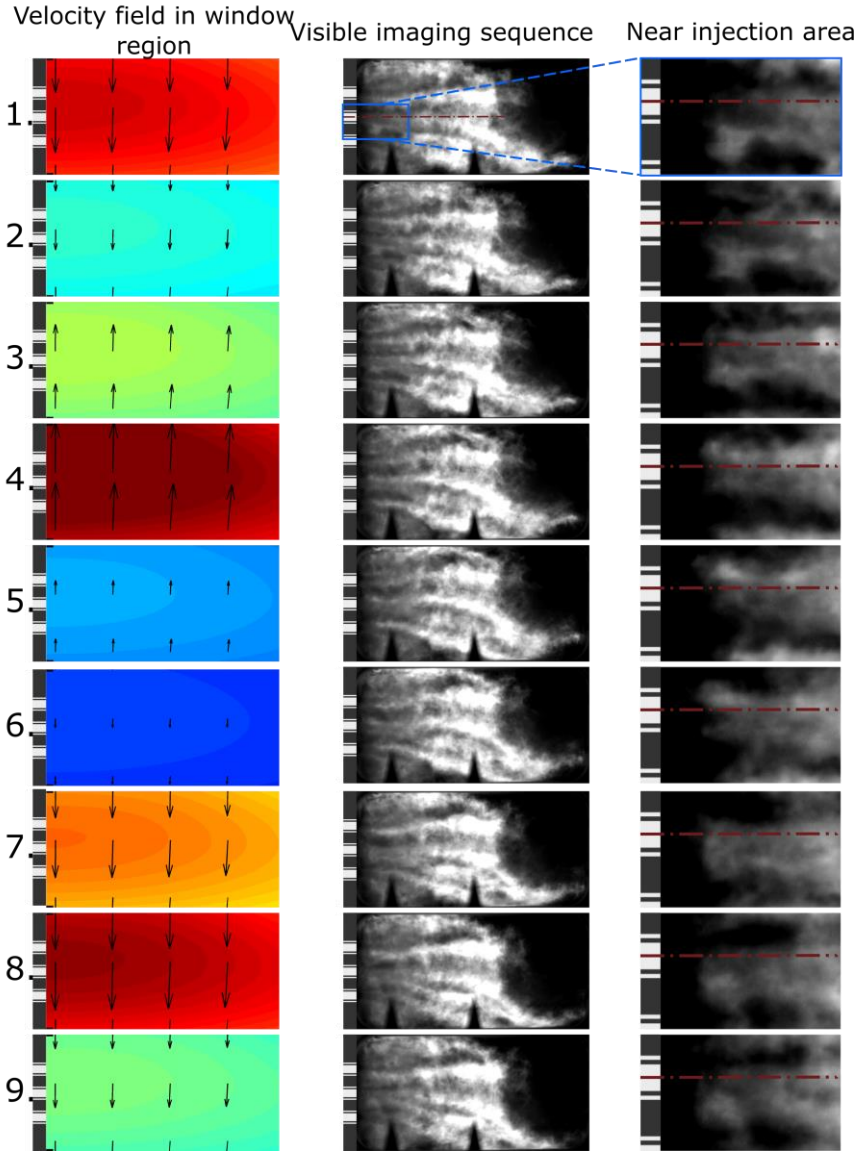

Figure 12: Constant excitation sequence image

Visualisation of the flame under continuous excitation is a valuable source of validation data. Identifying the spatial distribution of the flame and the spectral response of the flames under acoustic excitation has previously been presented [8,10,11]. VIS imaging of a flame under constant amplitude excitation has not previously been presented or analysed in detail. The added detail of VIS imaging which presents a composite image of flow field and flame zones could provide a new interface with numerical modelling results.

To investigate the spatial dependence of frequency response in VIS imaging, a number of points for analysis were selected (Figure 13). These points formed two rows. The upper row located on the edge of the flame (off oxygen jet axis) and corresponding to the points of high emission occurring above and below the frame as shown in Figure 12. The lower row is located just above the central axis on the oxygen jet (on oxygen jet axis). In both cases a 2 by 2 pixel region was averaged and a spectral analysis was made.

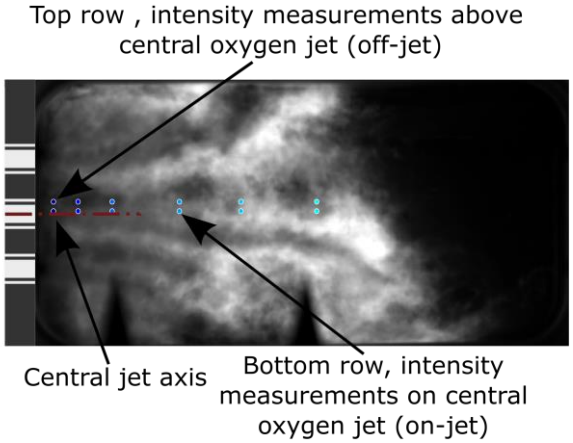

Figure 13: Points and full flame image

Figure 14 shows two columns of power density spectra. The first column corresponds to the on oxygen jet axis measurements and the second to the off oxygen jet axis measurements. The distance downstream from the faceplate is given for each power spectrum. The y-axis shows the amplitude per Hz in a logarithmic scale and the x-axis the frequency in kHz. In each image two peaks can be clearly identified. The first, corresponding to 4300 Hz, is the frequency of excitation. It is also the 1T-mode resonance frequency. The second peak is the first overtone of the 1T-mode at exactly twice the resonance frequency. It also corresponds to the frequency at which the magnitude of the velocity field is greatest, this occurs twice per 1T-mode oscillation, once in each vertical direction.

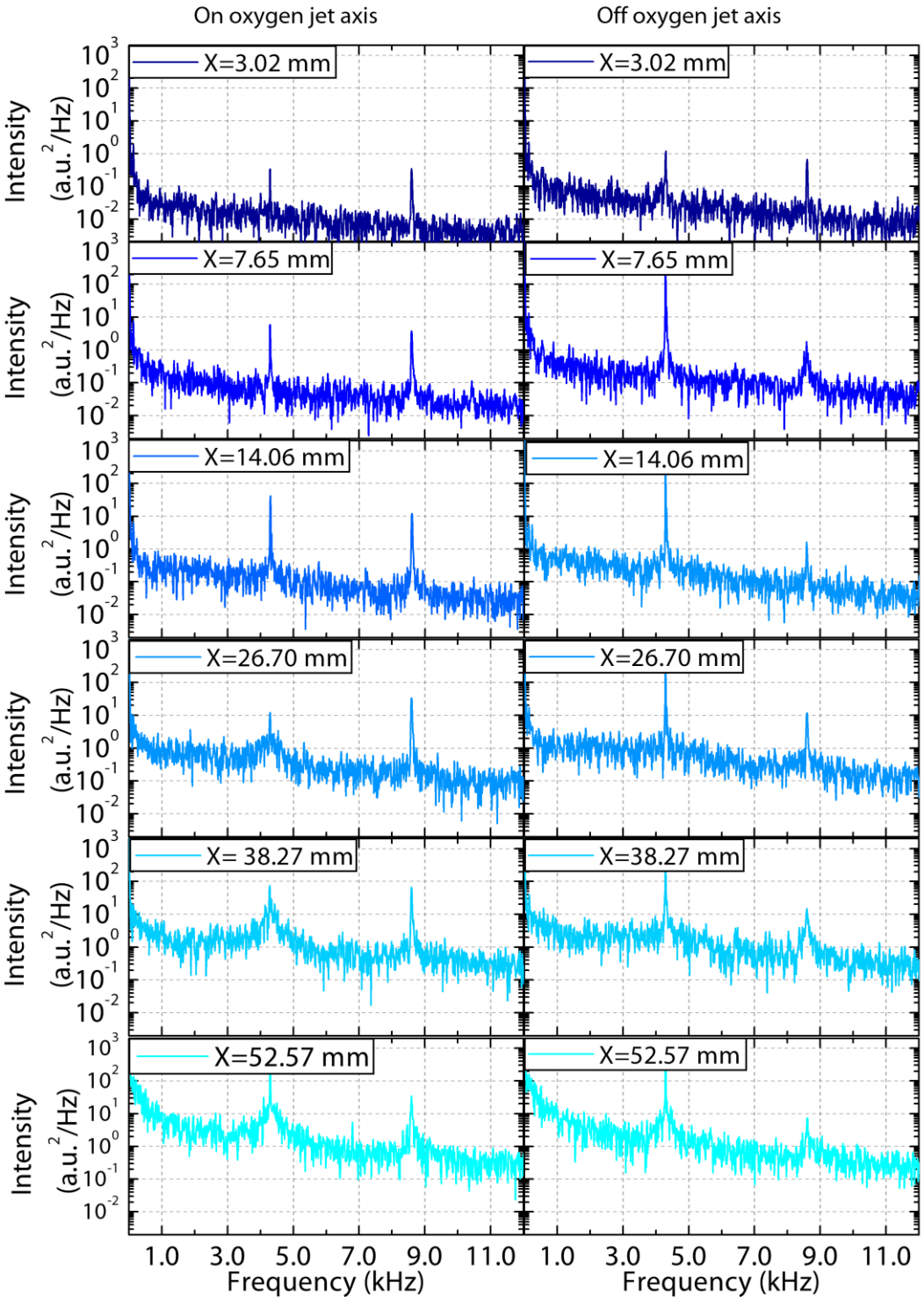

Figure 14: Frequency response at points in image.

The relative amplitude of the peaks as well as their width tells us about the flame behaviour. As the measurement point progresses downstream, the amplitude and width of the peaks increases, as does the amplitude of the background intensity. This is attributed to increased influence from turbulent structures on flame intensity measurements. In the on-axis spectra show both peaks have similar amplitudes for all distances from the face plate. This is not the case for the off-axis measurements where the first peak is always dominant. This suggests that the position with respect to the central jet is important when considering the frequency response of the flame intensity.

CONCLUSION

Visible spectrum imaging of flame response to two acoustic conditions has been presented. Imaging of the variable amplitude excitation shows the flame response to conditions representative of combustion instability onset where rapid amplitude increase occurs. The flame contracts and shows regions of improved combustion rate, represented by regions of high intensity, which form either side of the central oxygen jet. Both the flame and regions of high intensity contract toward the injection plane as the pressure and velocity amplitudes increase.

Under constant amplitude excitation the flame has reached a quasi-steady state length. The combustion on either side of the central oxygen core can be seen in the near injection plane. A frequency analysis of the flame response shows response at both the excitation frequency and double the excitation frequency. The influence of intensity oscillation due to turbulence can be observed in the width of the intensity response peaks and the amplitude of the background spectra, which increases with axial distance from the injection plane.

By using visible imaging the response of the flame to an acoustic field was observed. The response of the flame, both spatially and spectrally provides insight into the complex flame dynamics in a rocket combustor as well as providing valuable validation data for numerical simulation tools. In particular, the visualisation of the flame response under conditions analogous to combustion instability onset is unique.

REFERENCES

[1] Yang, V., & Anderson, W. Eds., (1995) *Liquid rocket engine combustion instability*, AIAA, Washington, D.C

[2] Harrje, D.T., & Reardon, F. H. (1972). *Liquid propellant rocket combustion instability*. NASA, Washington, D.C

[3] Zinn, Ben T. (1992). Pulse Combustion: Recent Applications and Research Issues. *Twenty-Fourth Symposium (International) on Combustion*. The Combustion Institute. 24:1297-1305.

[4] Rey, C., Ducruix S., Richecoeur, F., Scouflaire, P., Vingert, L., & Candel, S. (2004). High Frequency Combustion Instabilities Associated with Collective Interactions in Liquid Propulsion. AIAA/SAE/ASME/ASEE 40rd Joint Propulsion Conference.

[5] Cheuret, F. (2005). *Instabilitiès Thermo-Acoustiques de Combustion Haute-Fréquence dans les Moteurs Fusés. PhD Thesis,* Universitè de Provence- AIX Marseille I

[6] Richecoeur, F., Scouflaire, P., Ducruix, S. & Candel, S. (2006). High Frequency Transverse Acoustic Coupling in a Multiple Injector Cryogenic Combustor. *Journal of Propulsion and Power*. Vol 22. 4:790-799

[7] Hardi, J., Gomez Martinez, H., Oschwald, M., & Dally, B. (2012). Response of a reacting {Lox} jet to a transverse acoustic oscillation. Space Propulsion Conference. 7-10 May. Bordeaux, France.

[8] Hardi, J., Beinke, S., Oschwald, M. & Dally, B. (2014). Coupling of cryogenic oxygen-hydrogen flames to longitudinal and transverse acoustic instabilities. *Journal of Propulsion and Power*. Vol 30. 991-1004.

[9] Chehroudi, B., Talley, D., Mayer, W., Branam, R., Smith, J., Schik, A., & Oschwald, M. (2003). Understanding Injection into High Pressure Supercritical Environments. *5th International Symposium on Liquid Space Propulsion*.28-30 October. Chattanooga, Tennessee.

[10] Rey, C., Ducruix, P., Scouflaire, P., Vingert, L., & Candel. (2003). Experimental Analysis of High Frequency Combustion Instabilities associated with Collective Interactions. Proceedings of Pacific Symposium on Flow Visualisation and Imaging-4.3-5 June. Chamonix, France.

[11] Mery, Y., Hakim, L., Scouflaire, P., Vingert, L., Ducruix, S., & Candel, S. (2013). Experimental Investigation of Cryogenic Flame Dynamics Under Transvers Acoustic Modulations. *Comptes Rendus Mechanique*.1-2:100-109.

[12] Gaydon, A. (1957). *The Spectroscopy of Flames*. Chapman and Hall.

[13] Gaydon, A., and H. Wolfhard. (1978). *Flames: Their structure radiation and temperature*. John Wiley & Sons, Inc.

[14] Mayer, W. & Tamura, H. (1996). Propellant Injection in a Liquid Oxygen/Gaseous Hydrogen Rocket Engine. *Journal of Propulsion and Power*. 6:1137-1148.

[15] Smith, J., Schneider, G., Suslov, D., Oschwald, M. & Haiden, O. (2007). Steady-state high pressure Lox/H2 rocket engine combustion. Aerospace Science and Technology. Vol: 11. 1:39-47

[16] Koike, T. & Morinaga, K. (1982) Further studies of the rate constant for chemical excitation of OH in shock waves. *Bulletin of the Chemical society of Japan*. Vol: 55. 1:52-54.

[17] Fiala, T. & Sattelmayer, T. (2013). Heat Release and OH* Radiation in Laminar Non-Premixed Hydrogen-Oxygen Flames. 51st AIAA Aerospace Sciences Meeting including the New Horizons Forum and Aerospace Exposition. 7-10 January. Grapevine, Texas.

[18] Fiala, T. & Sattelmayer, T. (2013). On the Use of OH* Radiation as a Marker for the Heat Release Rate in High-Pressure Hydrogen-Oxygen Liquid Rocket Combustion. 49th AIAA/ASME/SAE/ASEE Joint Propulsion Conference 15-17 July. San Jose, California.

[19] Fiala, T., Nettinger, M., Rieger, F., Kumar, A. & Sattelmayer. (2014). Emission and absorption measurement in enclosed round jet flames. 16th International Symposium on Flow Visualisation.

[20] Fiala, T. (2015). *Radiation from High Pressure Hydrogen-Oxygen Flames and its Use in Assessing Rocket Combustion Instability*. PhD Thesis, Technische Universität München.

[21] Heidmann, M. F., & Wieber, P. R. (1966). Analysis of frequency response characteristics of propellant vaporization. NASA TN D-3749. Lewis Research Centre, National Aeronautics and Space Administration.

[22] Webster, S., Hardi, J., & Oschwald, M. (2014). High pressure visualisation of liquid oxygen and cryogenic hydrogen combustion under an imposed acoustic field. *Proceedings of the 19th Australasian Fluid Mechanics Conference*.Vol. CD-ROM, Australian Fluid Mechanics Society, PP 153:1-4